Nonsinusoidal angular dependence of FMR-driven spin current across an antiferromagnet in Y_{3}Fe_{5}O_{12}/NiO/Pt trilayers

Yang Cheng, Ricardo Zarzuela, Jack T. Brangham, Aidan J. Lee, Shane White, P. Chris Hammel, Yaroslav Tserkovnyak, and Fengyuan Yang

Phys. Rev. B **99**, 060405 — Published 11 February 2019

DOI: 10.1103/PhysRevB.99.060405

Non-sinusoidal angular dependence of FMR-driven spin current across an antiferromagnet in $Y_3Fe_5O_{12}$/NiO/Pt trilayers

Yang Cheng[1], Ricardo Zarzuela[2], Jack T. Brangham[1], Aidan J. Lee[1], Shane White[1], P. Chris Hammel[1], Yaroslav Tserkovnyak[2], Fengyuan Yang[1]

[1]Department of Physics, The Ohio State University, Columbus, Ohio 43210, USA

[1]Department of Physics and Astronomy, University of California, Los Angeles, California 90095, USA

Abstract

Out-of-plane angular (θ_H) dependence of inverse spin Hall effect (ISHE) voltage (V_{ISHE}) generated by spin pumping has been investigated in $Y_3Fe_5O_{12}$ (YIG)/NiO/Pt trilayers. A simple sinusoidal angular dependence of V_{ISHE} has been viewed as a signature of spin pumping. Surprisingly, we observe an extensive plateau in the V_{ISHE} vs. θ_H plots with a pronounced peak feature at $\theta_H \sim 45°$ to $60°$ when the measurement temperature is close to the Néel temperature (T_N) of NiO. This phenomenon can be understood as arising from the competition between the exchange coupling at the YIG/NiO interface, the easy-plane and in-plane easy-axis anisotropies of NiO, and the effect of the applied magnetic field. While insulating antiferromagnetic films can efficiently transmit spin currents and show promise for integration in spintronic devices, the underlying physics of spin ordering and dynamics is richer than currently understood.

Antiferromagnetic (AF) spintronics has generated intense interest in recent years [1-8] because AFs offer high frequency operations, ultra-low damping, and abundant choices of materials. One exciting discovery in this emerging field is the enhancement of pure spin currents with the insertion of a thin AF insulating layer between a ferromagnet (FM) and Pt, driven by either ferromagnetic resonance (FMR) spin pumping or a thermal gradient [9-14]. The spin conductance in AFs is optimal at temperatures (T) near the AF ordering temperature, referred to as T_N here [12, 14, 15]. Several theories have been proposed to explain the high efficiency of AF spin transport [13, 16-18]. However, a full understanding of the thin-film AF ordering and its interaction with adjacent materials remains an open problem in AF spintronics, which envisions using AFs as a spin conduit. We investigate AF spin transport by measuring their transmission of a spin-pumping signal, while controlling the strength of the AF order and its orientation.

In this Letter, we report a study of the out-of-plane angular dependence of spin pumping signals (V_{ISHE}) in YIG/NiO/Pt trilayers, which exhibit an unusual non-sinusoidal dependence. We find that for NiO thicknesses of 5 to 10 nm at room temperature (RT), as the applied field ($\boldsymbol{H}$) rotates from in-plane towards out-of-plane, V_{ISHE} surprisingly increases initially and peaks at a field angle of $\theta_H \sim 45°$ to 60°, then decreases sharply and changes sign. We ascribe this behavior to the spin-current modulation by the AF, resulting from the interplay between the interfacial exchange interaction and the easy-plane, in-plane easy-axis, and field-induced anisotropies in NiO.

YIG(35 nm)/NiO(t_{NiO})/Pt(5 nm) trilayers were deposited using off-axis sputtering on $Gd_3Ga_5O_{12}$ (GGG) (111) substrates [19]. (111)-textured NiO layers with thicknesses from 0.5 to 40 nm were grown at RT [10]. Figure 1a shows a FMR derivative absorption spectrum taken in a cavity at a radio frequency (rf) f_{rf} = 9.4 GHz and microwave power P_{rf} = 0.2 mW, which gives

a peak-to-peak linewidth of 3.1 Oe. The samples of ~1 mm × 5 mm are put into the cavity with a dc field $\boldsymbol{H}$ applied in the *xz* plane at an angle of θ_H relative to the *x*-axis, while the ISHE voltage is measured along the long edge (*y*-axis) of the films (see Fig. 1b). For a YIG/Pt bilayer in the presence of an in-plane dc field ($\boldsymbol{H}$ || *x*-axis) and an rf field (h_{rf}), the precessing YIG magnetization ($\boldsymbol{M}$) generates a pure spin current $\boldsymbol{j_s}$ (|| *z*-axis) in Pt [20]. Figure 1c shows a representative V_{ISHE} vs. H - H_{res} spectrum at $\theta_H = 0°$ for a YIG/Pt bilayer, where H_{res} is the resonance field. The very large V_{ISHE} = 2.38 mV provides a dynamic range of four orders of magnitude for this study. Since for YIG $4\pi M_s < H_{res}$ and $\boldsymbol{M}$ essentially follows (but lags behind) $\boldsymbol{H}$, a (quasi-)sinusoidal dependence of V_{ISHE} on θ_H is expected, which is regarded as a signature of spin pumping [19].

Spin pumping measurements on the YIG/NiO/Pt trilayers were performed in the cavity using a flow cryostat. Figure 1d shows the temperature dependence of normalized V_{ISHE} for trilayers with 2, 5, and 10 nm NiO. A peak is observed for the 2 nm and 5 nm NiO samples at 220 and 260 K, respectively, while the curve for the 10 nm NiO sample increases monotonically up to the highest accessible temperature of 300 K, suggesting a peak above RT. This agrees with previous reports that the peak spin current occurs near T_N [12, 14, 15].

Figure 2 shows the angular dependences (θ_H) of V_{ISHE} for trilayers with t_{NiO} from 0 to 20 nm at RT, where the ISHE voltages are normalized by the values at $\theta_H = 0°$. The YIG/Pt bilayer (t_{NiO} = 0 nm) exhibits the expected sinusoidal behavior. As t_{NiO} increases from 0.5 to 2 nm, the curves show clear deviation from the sinusoidal behavior. At t_{NiO} = 5 and 10 nm, a qualitatively distinct, counterintuitive feature emerges: from $\theta_H = 0°$ to 60° (and from 360° to 315°), V_{ISHE} increases with θ_H and peaks at $\theta_H = 60°$ (and 315°). After peaking, V_{ISHE} quickly decreases and reverses sign, then plateaus between ~135° and 240° (with peaks at both ends of the plateau). At

t_{NiO} = 15 nm, the angular dependence returns towards the sinusoidal behavior and at t_{NiO} = 20 nm, the data can be described nicely by a cosine function again. To illustrate how the non-sinusoidal behavior evolves with t_{NiO}, we plot the normalized V_{ISHE} at θ_H = 60° as a function of t_{NiO} in the inset of Fig. 2, which increases from 0.58 (note cos60° = 0.5) at t_{NiO} = 0 nm to 1.26 at t_{NiO} = 10 nm before falling back to 0.67 above t_{NiO} = 15 nm. The enhancement of V_{ISHE} at θ_H = 60° indicates that unusual AF spin structures in NiO significantly impact the spin conduction.

We note that T_N's for the 5 and 10 nm NiO are close to RT (Fig. 1d), suggesting the important role of AF fluctuations in spin transport. Figure 3a shows the V_{ISHE} vs. θ_H curves from 293 down to 80 K for the YIG/NiO(5 nm)/Pt trilayer. As T decreases from RT, the plateaus and the peaks become less pronounced and the data returns to sinusoidal at low temperatures, *e.g.*, 80 K, where the AF ordering is stronger. The trilayers with 2 and 10 nm NiO (Figs. 3b and 3c) exhibit clear plateaus at RT, but becomes sinusoidal at low temperatures. For the 0.5 nm and 20 nm NiO (Fig. 3d) samples, the angular dependence follows the cosine function at all temperatures.

Altogether, the unusual angular dependence indicates the important role of NiO in spin conduction. NiO has a bulk T_N = 525 K [21], but for the 5 and 10 nm NiO, T_N can be near RT [22], which exhibit the intriguing non-sinusoidal dependence. The peaks in Figs. 2 and 3 show an optimal spin transport with $\boldsymbol{H}$ applied at θ_H = 45° to 60° (or 300° to 315°), instead of at θ_H = 0°. For very thin NiO (*e.g.*, 0.5 nm) with very low T_N, and very thick NiO (*e.g.*, 20 nm) with T_N well above RT, the angular dependence follows the cosine function in the whole temperature range.

Our results suggest that the AF order and correlations in the NiO layer near T_N are essential for the understanding of the surprising angular dependence of V_{ISHE}. We propose the

following phenomenological model to describe the main features of the results. Given that $4\pi M_s \approx 1800$ G as compared to H_{res} ~2500 - 5500 Oe for YIG, $\boldsymbol{M} \propto (\cos\theta_M, 0, \sin\theta_M)$ essentially follows, but in general lags behind $\boldsymbol{H} \propto (\cos\theta_H, 0, \sin\theta_H)$. The lagging angle $\theta_H - \theta_M$ can be calculated by minimizing the free energy of the YIG layer, which includes Zeeman and demagnetizing terms; it becomes zero at $\theta_H = 0°$ and 90°, but reaches its maximum value of 15° near $\theta_H \sim 50°$. Since the spin polarization $\boldsymbol{\sigma} \,||\, \boldsymbol{M}$, $\boldsymbol{j_s} \,||\, \hat{\boldsymbol{z}}$, and $V_{ISHE} \propto \hat{\boldsymbol{y}} \cdot (\boldsymbol{j_s} \times \boldsymbol{\sigma})$,

$$V_{ISHE} \propto \boldsymbol{m} \cdot \hat{\boldsymbol{x}} = \cos\theta_M, \tag{1}$$

where $\boldsymbol{m} = \boldsymbol{M}/|\boldsymbol{M}|$, $\hat{\boldsymbol{x}}$, $\hat{\boldsymbol{y}}$, and $\hat{\boldsymbol{z}}$ are unit vectors describing the YIG magnetization and the coordinate axes, respectively. Eq. (1) gives an approximately sinusoidal V_{ISHE} vs. θ_H dependence. However, for the YIG/NiO/Pt trilayers, the AF spins modulate $\boldsymbol{j_s}$ and V_{ISHE} as described by

$$V_{ISHE} \propto (\boldsymbol{m} \cdot \boldsymbol{n})(\boldsymbol{n} \cdot \hat{\boldsymbol{x}}), \tag{2}$$

where $\boldsymbol{n}$ is the unit vector along the Néel order of NiO. The factor $(\boldsymbol{m} \cdot \boldsymbol{n})$ reflects a spin flow from YIG into NiO, while $(\boldsymbol{n} \cdot \hat{\boldsymbol{x}})$ is dictated by the ISHE detection of spin pumping from NiO into Pt. The interplay of the geometric factors $(\boldsymbol{m} \cdot \boldsymbol{n})$ and $(\boldsymbol{n} \cdot \hat{\boldsymbol{x}})$ is responsible for the non-sinusoidal behavior. Assuming that both YIG and NiO are in the monodomain state, we obtain the free energy,

$$E(\boldsymbol{m}, \boldsymbol{n}) = -J\boldsymbol{m} \cdot \boldsymbol{n} + \frac{K_1}{2}(\boldsymbol{n} \cdot \hat{\boldsymbol{z}})^2 - \frac{K_2}{2}(\boldsymbol{n} \cdot \hat{\boldsymbol{x}})^2 + \frac{N}{2}(\boldsymbol{h} \cdot \boldsymbol{n})^2. \tag{3}$$

The first term arises from the exchange coupling (J) at the YIG/NiO interface, while the second and the third are due to the easy-plane (111) anisotropy (K_1) and in-plane easy-axis (along $\hat{\boldsymbol{x}}$) anisotropy (K_2) of NiO. The last term is the field-induced hard-axis anisotropy in NiO: $N \sim \chi H^2$, where χ is the transverse spin susceptibility, and $\boldsymbol{h} = \boldsymbol{H}/|\boldsymbol{H}|$ is the unit vector along $\boldsymbol{H}$. This

term favors $\boldsymbol{n} \perp \boldsymbol{H}$ and is responsible for the spin-flop transition [23, 24]. Eq. (3) can be recast as

$$E(\boldsymbol{m}, \boldsymbol{n}) = -c\boldsymbol{m} \cdot \boldsymbol{n} + \frac{k_1}{2}(\boldsymbol{n} \cdot \hat{\boldsymbol{z}})^2 - \frac{k_2}{2}(\boldsymbol{n} \cdot \hat{\boldsymbol{x}})^2 + \frac{1}{2}(\boldsymbol{h} \cdot \boldsymbol{n})^2, \quad (4)$$

where $c = J/N$ and $k_{1,2} = K_{1,2}/N$. We note that J, K_1, K_2, and N are effective coarse-grained parameters that can depend on the AF thickness, temperature, and growth conditions [25, 26].

For very thick NiO (*e.g.*, 20 nm), $T_N > T$ and the AF ordering is robust. Because of its strong easy-plane anisotropy, the NiO spins remain in plane regardless of the field angle θ_H (see Fig. 4a). As a result, only the in-plane component of the spin polarization carried by $\boldsymbol{j_s}$ can be conducted across the NiO layer and reaches the NiO/Pt interface to generate an ISHE signal [27, 28]. In this case, $(\boldsymbol{n} \cdot \hat{\boldsymbol{x}}) = 1$ and Eq. (2) is simplified to Eq. (1), resulting in the same sinusoidal dependence as for the YIG/Pt bilayer. For very thin NiO films (*e.g.*, 0.5 nm), where $T_N << T$, the long-range AF order breaks down and NiO behaves as a paramagnet with AF correlations. The NiO spins follow the YIG magnetization (lagging behind $\boldsymbol{H}$) as shown in Fig. 4b. Thus, $(\boldsymbol{m} \cdot \boldsymbol{n}) = 1$ and Eq. (2) becomes $V_{ISHE} \propto (\boldsymbol{n} \cdot \hat{\boldsymbol{x}}) \propto \cos\theta_M$, resulting in the sinusoidal dependence.

For intermediate NiO thicknesses ($T \sim T_N$) the AF correlations remain strong but the AF spins start to respond to $\boldsymbol{H}$. Although the spin-flop field (H_{SF}) is several Tesla or higher in AF-ordered NiO, H_{SF} vanishes at T_N [29]. At $T \sim T_N$, the NiO layer should have undergone spin-flop transition at H_{res} and its Néel vector deviates from $\boldsymbol{H}$. The AF configuration and its impact on the spin current can be derived by minimizing the energy in Eq. (4). Below we split the angular range into two sectors: $0 < \theta_H < \theta_c$ and $\theta_c < \theta_H < \frac{\pi}{2}$, where θ_c represents the critical angle at which the AF spins change from staying in plane at $\theta_H < \theta_c$ to out-of-plane at $\theta_H > \theta_c$.

A. $0 < \theta_H < \theta_c$. In this sector, $\boldsymbol{n}$ lies in the *xy* plane (n_z = 0) for strong easy-plane anisotropy and Eq. (4) reduces to $E(\boldsymbol{n}) = -c \cdot \cos\theta_M n_x + \frac{\cos^2\theta_H - k_2}{2} n_x^2$. Energy minimization

yields $n_x = c\frac{\cos\theta_M}{(\cos^2\theta_H - k_2)}$, from which we obtain the implicit equation $c\frac{\cos\theta_M}{(\cos^2\theta_c - k_2)} = 1$ for the critical angle. As a result, $V_{ISHE}(\theta_H) \propto m_x n_x^2 = \frac{c^2\cos^3\theta_M}{(\cos^2\theta_H - k_2)^2}$. By choosing the appropriate values for c and k_2, $V_{ISHE}(\theta_H)$ increases monotonically with θ_H in this range. Given $N \sim \chi H^2$, c, k_1, and k_2 are all field dependent; thus, we redefine $c = c_0 H_{res}^2(\theta_H = 0)/H_{res}^2(\theta_H)$, $k_1 = k_{1,0} H_{res}^2(\theta_H = 0)/H_{res}^2(\theta_H)$, and $k_2 = k_{2,0} H_{res}^2(\theta_H = 0)/H_{res}^2(\theta_H)$, where $c_0, k_{1,0}, k_{2,0}$ are field-independent fitting parameters.

B. $\theta_c < \theta_H < \frac{\pi}{2}$. Here, we find that the AF order lies in the *xz* plane (see Fig. 4d). The energy in Eq. (4) can be recast in terms of $\boldsymbol{n} = (n_x, 0, n_z)$ as

$$E(\boldsymbol{n}) = -c(\cos\theta_M n_x + \sin\theta_M n_z) + \frac{k_1}{2} n_z^2 - \frac{k_2}{2} n_x^2 + \frac{1}{2}(\cos\theta_H n_x + \sin\theta_H n_z)^2 \equiv$$

$$-c\left(\cos\theta_M n_x + \sin\theta_M \sqrt{1 - n_x^2}\right) - \frac{k_1 + k_2 - \cos(2\theta_H)}{2} n_x^2 + \frac{1}{2}\sin(2\theta_H)\, n_x \sqrt{1 - n_x^2}. \quad (5)$$

By minimizing Eq. (5) over n_x, we obtain V_{ISHE} which decreases monotonically with θ_H from $\theta_H = \theta_c$ to $\frac{\pi}{2}$, where it changes sign.

We test our model by fitting the 10 nm NiO data at 293 K as plotted in Fig. 5a, where the fitting curve uses c_0 = 0.5, $k_{1,0}$ = 15, and $k_{2,0}$ = 0.35, which result in θ_c = 58°. The ratio of $k_{1,0}/k_{2,0}$ = 43 reflects the fact that the out-of-plane anisotropy is much stronger than the in-plane one [30]. The fit captures accurately the main features, including the peak at $\theta_H = 45°$ to 60° and the sign switching at 90°. The fitting curves of $V_{ISHE}(\theta_H)$ depend on the parameters $c_0, k_{1,0}, k_{2,0}$ (and consequently, θ_c). In Fig. 5b, we fix c_0 = 0.5 and $k_{1,0}$ = 15 while varying $k_{2,0}$ from 0.05 to 0.45 (θ_c from 76° to 45°); in Fig. 5c, we fix $k_{1,0}$ = 15 and $k_{2,0}$ = 35 while c_0 varies from 0.35 to 0.55 (θ_c from 64° to 54°), both of which exhibit a shift in the peak positions as well as the enhancement ratio.

In this model, the competition between the exchange coupling at the YIG/NiO interface,

which tries to orient the Néel order along $\boldsymbol{M}$, and the spin-flop tendency inside NiO, which tries to orient the AF order perpendicular to $\boldsymbol{H}$, together with the easy-plane and in-plane easy-axis anisotropies, which tries to orient the AF spins along $\hat{\boldsymbol{x}}$, gives rise to the surprising non-sinusoidal dependence and peaks at $\theta_H = 45°$ to 60°. It should be pointed out that we assume the Néel order in NiO to be uniform along a single orientation ($\boldsymbol{n}$). In reality, the AF spin structure could be more complicated. For example, the AF spins may form a spiral near the YIG/NiO interface due to the competition between the interfacial exchange coupling and the easy-plane AF anisotropy [31].

In summary, we observe an unusual angular dependence of spin pumping signals in YIG/NiO/Pt trilayers. For intermediate NiO thicknesses (5 and 10 nm) with $T \sim T_N$, a peak emerges in the V_{ISHE} vs. θ_H spectra at θ_H = 45° to 60°. We propose a model which accurately reproduces the key features of the experimental data. This agreement suggests that at $T \sim T_N$, where AF spin transport is optimal, the AF spin configuration is determined by the interplay among the interfacial exchange coupling, the easy-plane anisotropy, the in-plane easy-axis anisotropy, and the field-induced hard-axis anisotropy, leading to a non-sinusoidal angular dependence. This result broadens our understanding of the role and behavior of AF spins in dynamic spin transport, which may have important implications in the development of AF-based spintronics.

This work was supported primarily by the Center for Emergent Materials, an NSF MRSEC, under Grant No. DMR-1420451 (YC, AJL, PCH, and YT) and the U.S. Department of Energy (DOE) under Grant No. DE-SC0001304 (JTB and FYY), and partially supported by DOE under Grant No. DE-FG02-03ER46054 (SW) and NSF under Grant No. DMR-1742928 (RZ).

Figure Captions:

Figure 1. (a) FMR derivate absorption spectrum of a 35 nm YIG measured at room temperature in a cavity at f_{rf} = 9.4 GHz and P_{rf} = 0.2 mW. (b) Schematic of ISHE experimental setup and the coordinate system. (c) V_{ISHE} vs. H - H_{res} spectrum for a YIG(35 nm)/Pt(5 nm) bilayer at P_{rf} = 200 mW. (d) Normalized in-plane V_{ISHE} (θ_H = 0°) as a function of temperature for YIG/NiO/Pt trilayers with 2, 5, and 10 nm NiO. The peak position indicates the T_N for different t_{NiO}.

Figure 2. Normalized V_{ISHE} as a function of θ_H for YIG(35 nm)/NiO(t_{NiO})/Pt(5 nm) trilayers, where t_{NiO} ranges from 0 to 20 nm. The t_{NiO} = 0 and 20 nm curves are fit by a cosine function. Inset: V_{ISHE} (θ_H = 60°) normalized by V_{ISHE} (θ_H = 0°) as a function of t_{NiO}. Curves are shifted vertically for clarity.

Figure 3. Normalized V_{ISHE} vs. θ_H for YIG(35 nm)/NiO(t_{NiO})/Pt(5 nm) trilayers with (a) t_{NiO} = 5 nm, (b) t_{NiO} = 2 nm, (c) t_{NiO} = 10 nm, and (d) t_{NiO} = 20 nm at different temperatures. Angular dependence curves at the lowest temperature are fit by a cosine function. Each V_{ISHE} curve is normalized by V_{ISHE} (θ_H = 0°).

Figure 4. AF spin configurations of NiO in YIG/NiO/Pt trilayers at (a) $T << T_N$ for a thick NiO layer, (b) $T >> T_N$ for a very thin NiO layer, and $T \sim T_N$ for intermediate NiO thicknesses at angular range of (c) $0 < \theta_H < \theta_c$ and (d) $\theta_c < \theta_H < \frac{\pi}{2}$. Note the Néel order in NiO is in the *xz* plane in (a), (b), and (d), but is in the *xy* plane (not along the *x*-axis) in (c).

Figure 5. (a) Modeling of the angular dependence of V_{ISHE} for the 10 nm NiO sample measured at 293 K. Red dots are the experimental data and the black curve is the fitting curve with parameters c_0 = 0.5, $k_{1,0}$ = 15, and $k_{2,0}$ = 0.35, which result in θ_c = 58°. Angular dependence of the calculated V_{ISHE} for (b) c_0 = 0.5 and $k_{1,0}$ = 15 with different values of $k_{2,0}$ and θ_c, and (c) $k_{1,0}$ = 15 and $k_{2,0}$ = 0.35 with different values of c_0 and θ_c.

References:

1. T. Kampfrath, A. Sell, G. Klatt, A. Pashkin, S. Mahrlein, T. Dekorsy, M. Wolf, M. Fiebig, A. Leitenstorfer and R. Huber, *Nat. Photonics* **5**, 31 (2011).
2. A. H. MacDonald and M. Tsoi, *Phil. Trans. Roy. Soc. A-Math. Phys. Eng. Sci.* **369**, 3098 (2011).
3. R. Cheng, J. Xiao, Q. Niu and A. Brataas, *Phys. Rev. Lett.* **113**, 057601 (2014).
4. S. Takei, B. I. Halperin, A. Yacoby and Y. Tserkovnyak, *Phys. Rev. B* **90**, 094408 (2014).
5. T. Jungwirth, X. Marti, P. Wadley and J. Wunderlich, *Nat. Nanotechnol.* **11**, 231 (2016).
6. X. Marti, I. Fina, C. Frontera, J. Liu, P. Wadley, Q. He, R. J. Paull, J. D. Clarkson, J. Kudrnovsky, I. Turek, J. Kunes, D. Yi, J. H. Chu, C. T. Nelson, L. You, E. Arenholz, S. Salahuddin, J. Fontcuberta, T. Jungwirth and R. Ramesh, *Nat. Mater.* **13**, 367 (2014).
7. P. Wadley, B. Howells, J. Zelezny, C. Andrews, V. Hills, R. P. Campion, V. Novak, K. Olejnik, F. Maccherozzi, S. S. Dhesi, S. Y. Martin, T. Wagner, J. Wunderlich, F. Freimuth, Y. Mokrousov, J. Kunes, J. S. Chauhan, M. J. Grzybowski, A. W. Rushforth, K. W. Edmonds, B. L. Gallagher and T. Jungwirth, *Science* **351**, 587 (2016).
8. V. Baltz, A. Manchon, M. Tsoi, T. Moriyama, T. Ono and Y. Tserkovnyak, *Rev. Mod. Phys.* **90**, 015005 (2018).
9. C. Hahn, G. De Loubens, V. V. Naletov, J. Ben Youssef, O. Klein and M. Viret, *Europhys. Lett.* **108**, 57005 (2014).
10. H. L. Wang, C. H. Du, P. C. Hammel and F. Y. Yang, *Phys. Rev. Lett.* **113**, 097202 (2014).
11. H. L. Wang, C. H. Du, P. C. Hammel and F. Y. Yang, *Phys. Rev. B* **91**, 220410(R) (2015).
12. W. W. Lin, K. Chen, S. F. Zhang and C. L. Chien, *Phys. Rev. Lett.* **116**, 186601 (2016).
13. S. A. Bender, H. Skarsvag, A. Brataas and R. A. Duine, *Phys. Rev. Lett.* **119**, 056804 (2017).
14. Z. Qiu, J. Li, D. Hou, E. Arenholz, A. T. N'Diaye, A. Tan, K.-i. Uchida, K. Sato, S. Okamoto, Y. Tserkovnyak, Z. Q. Qiu and E. Saitoh, *Nat. Commun.* **7**, 12670 (2016).
15. A. Prakash, J. Brangham, F. Y. Yang and J. P. Heremans, *Phys. Rev. B* **94**, 014427 (2016).
16. S. M. Rezende, R. L. Rodriguez-Suarez and A. Azevedo, *Phys. Rev. B* **93**, 014425 (2016).
17. K. Chen, W. Lin, C. L. Chien and S. Zhang, *Phys. Rev. B* **94**, 054413 (2016).
18. R. Khymyn, I. Lisenkov, V. S. Tiberkevich, A. N. Slavin and B. A. Ivanov, *Phys. Rev. B* **93**, 224421 (2016).
19. F. Y. Yang and P. C. Hammel, *J. Phys. D: Appl. Phys.* **51**, 253001 (2018).
20. K. Ando, S. Takahashi, J. Ieda, Y. Kajiwara, H. Nakayama, T. Yoshino, K. Harii, Y. Fujikawa, M. Matsuo, S. Maekawa and E. Saitoh, *J. Appl. Phys.* **109**, 103913 (2011).
21. W. L. Roth, *Phys. Rev.* **110**, 1333 (1958).
22. A. J. Devasahayam and M. H. Kryder, *J. Appl. Phys.* **85**, 5519 (1999).
23. S. Seki, T. Ideue, M. Kubota, Y. Kozuka, R. Takagi, M. Nakamura, Y. Kaneko, M. Kawasaki and Y. Tokura, *Phys. Rev. Lett.* **115**, 266601 (2015).
24. S. M. Wu, W. Zhang, K. C. Amit, P. Borisov, J. E. Pearson, J. S. Jiang, D. Lederman, A. Hoffmann and A. Bhattacharya, *Phys. Rev. Lett.* **116**, 097204 (2016).
25. L. Baldrati, A. Ross, T. Niizeki, C. Schneider, R. Ramos, J. Cramer, O. Gomonay, M. Filianina, T. Savchenko, D. Heinze, A. Kleibert, E. Saitoh, J. Sinova and M. Klaui, *Phys. Rev. B* **98**, 024422 (2018).
26. A. P. Malozemoff, *Phys. Rev. B* **35**, 3679 (1987).
27. Z. Y. Qiu, D. Z. Hou, J. Barker, K. Yamamoto, O. Gomonay and E. Saitoh, *Nat. Mater.* **17**, 577 (2018).
28. S. K. Kim, Y. Tserkovnyak and O. Tchernyshyov, *Phys. Rev. B* **90**, 104406 (2014).

29. F. L. A. Machado, P. R. T. Ribeiro, J. Holanda, R. L. Rodríguez-Suárez, A. Azevedo and S. M. Rezende, *Phys. Rev. B* **95**, 104418 (2017).
30. T. Satoh, S. J. Cho, R. Iida, T. Shimura, K. Kuroda, H. Ueda, Y. Ueda, B. A. Ivanov, F. Nori and M. Fiebig, *Phys. Rev. Lett.* **105**, 077402 (2010).
31. F. Y. Yang and C. L. Chien, *Phys. Rev. Lett.* **85**, 2597 (2000).

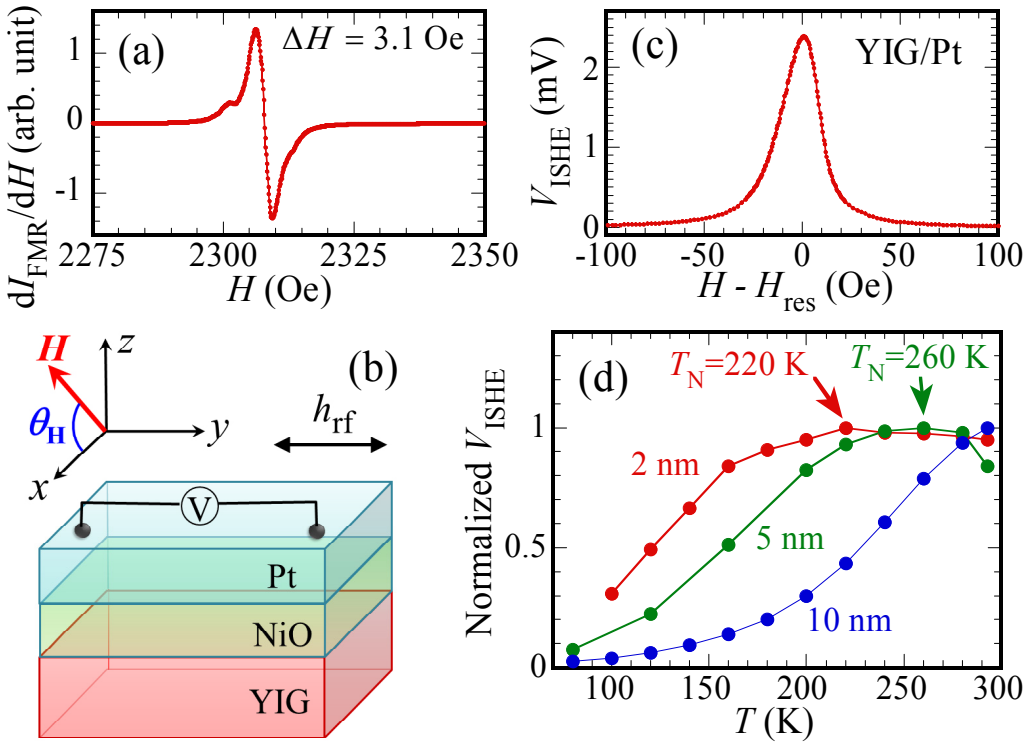
(a)
ΔH = 3.1 Oe
dI_FMR/dH (arb. unit)
H (Oe)
(c)
YIG/Pt
V_ISHE (mV)
H - H_res (Oe)
(b)
H
θ_H
z
y
x
h_rf
V
Pt
NiO
YIG
(d)
T_N=220 K
T_N=260 K
2 nm
5 nm
10 nm
Normalized V_ISHE
T (K)

Figure 1.

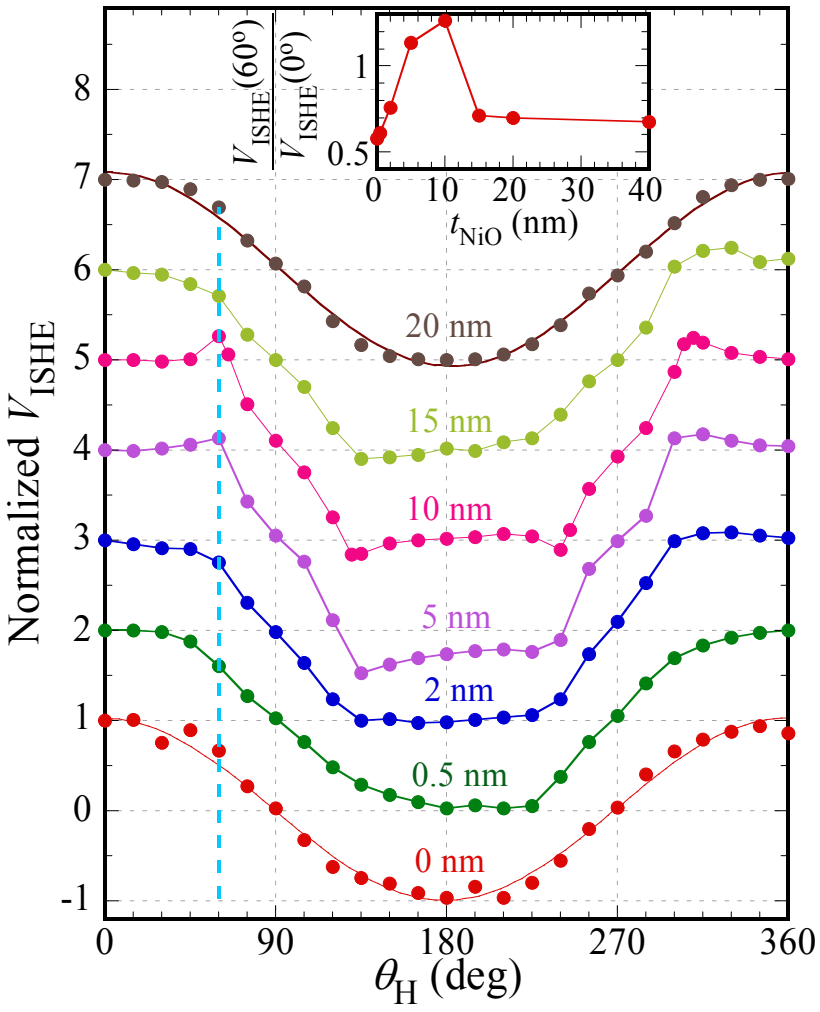
Normalized V_{ISHE}
θ_H (deg)
0
90
180
270
360
-1
0
1
2
3
4
5
6
7
8
20 nm
15 nm
10 nm
5 nm
2 nm
0.5 nm
0 nm
$\frac{V_{ISHE}(60^o)}{V_{ISHE}(0^o)}$
0.5
1
0
10
20
30
40
t_{NiO} (nm)

Figure 2.

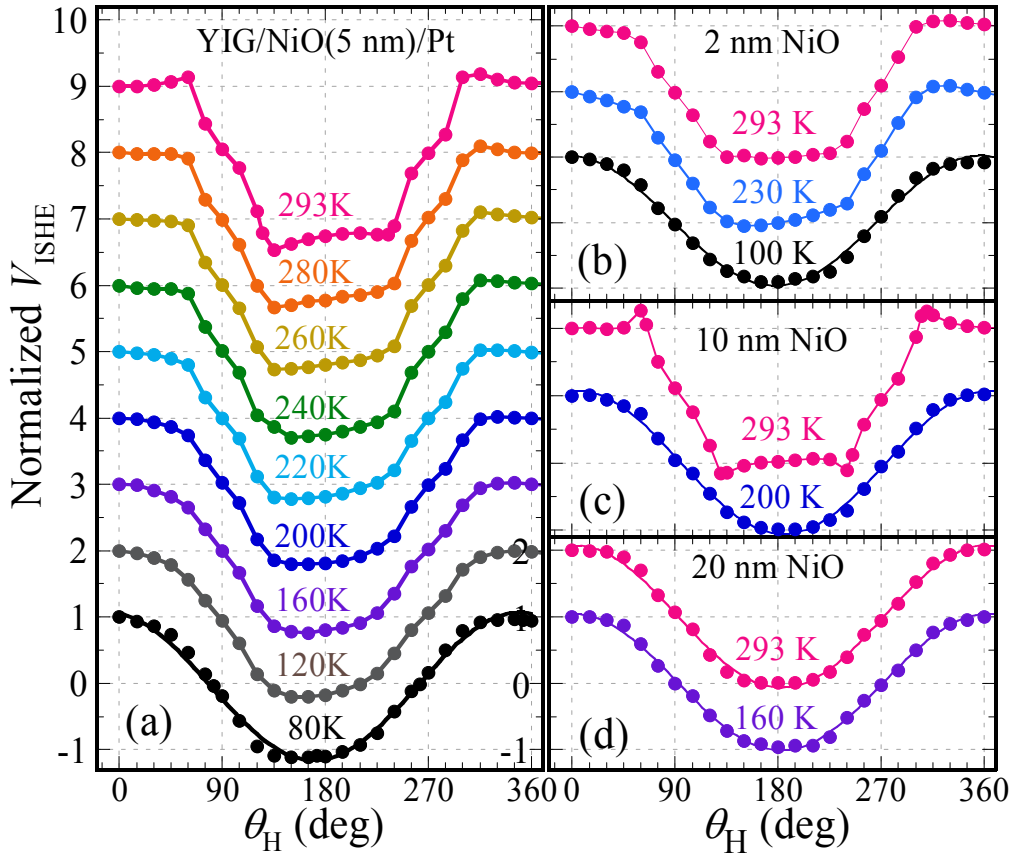
YIG/NiO(5 nm)/Pt
293K
280K
260K
240K
220K
200K
160K
120K
80K
(a)
Normalized V_{ISHE}
θ_H (deg)
2 nm NiO
293 K
230 K
100 K
(b)
10 nm NiO
293 K
200 K
(c)
20 nm NiO
293 K
160 K
(d)

Figure 3.

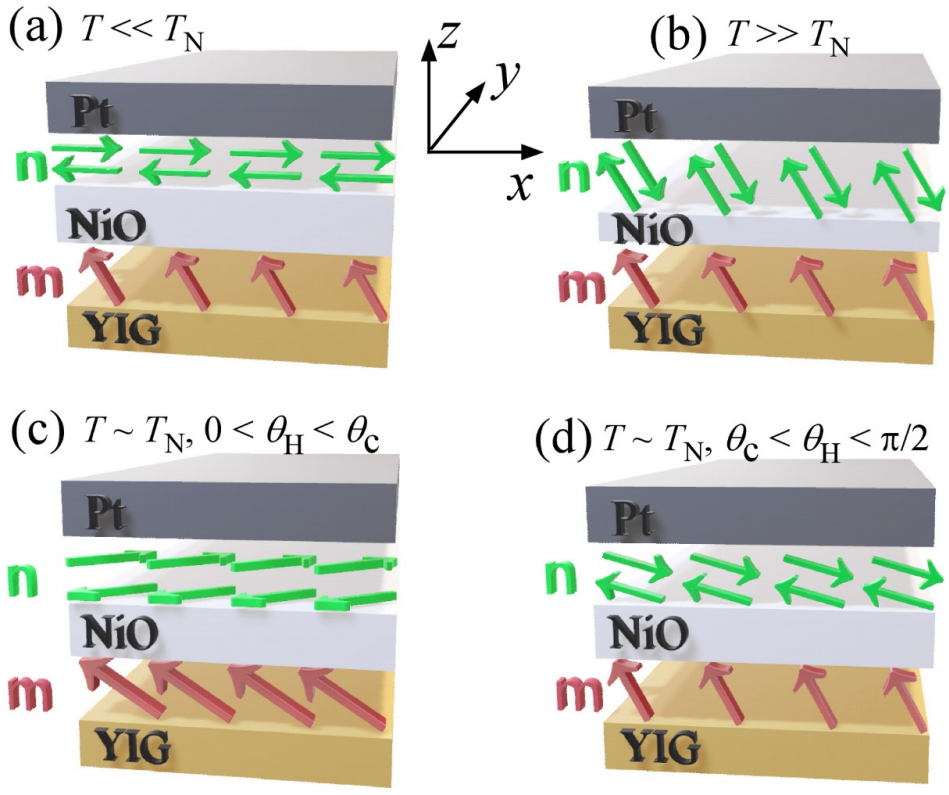
(a) $T << T_N$
(b) $T >> T_N$
(c) $T \sim T_N$, $0 < \theta_H < \theta_c$
(d) $T \sim T_N$, $\theta_c < \theta_H < \pi/2$
z
y
x
Pt
NiO
YIG
n
m

Figure 4.

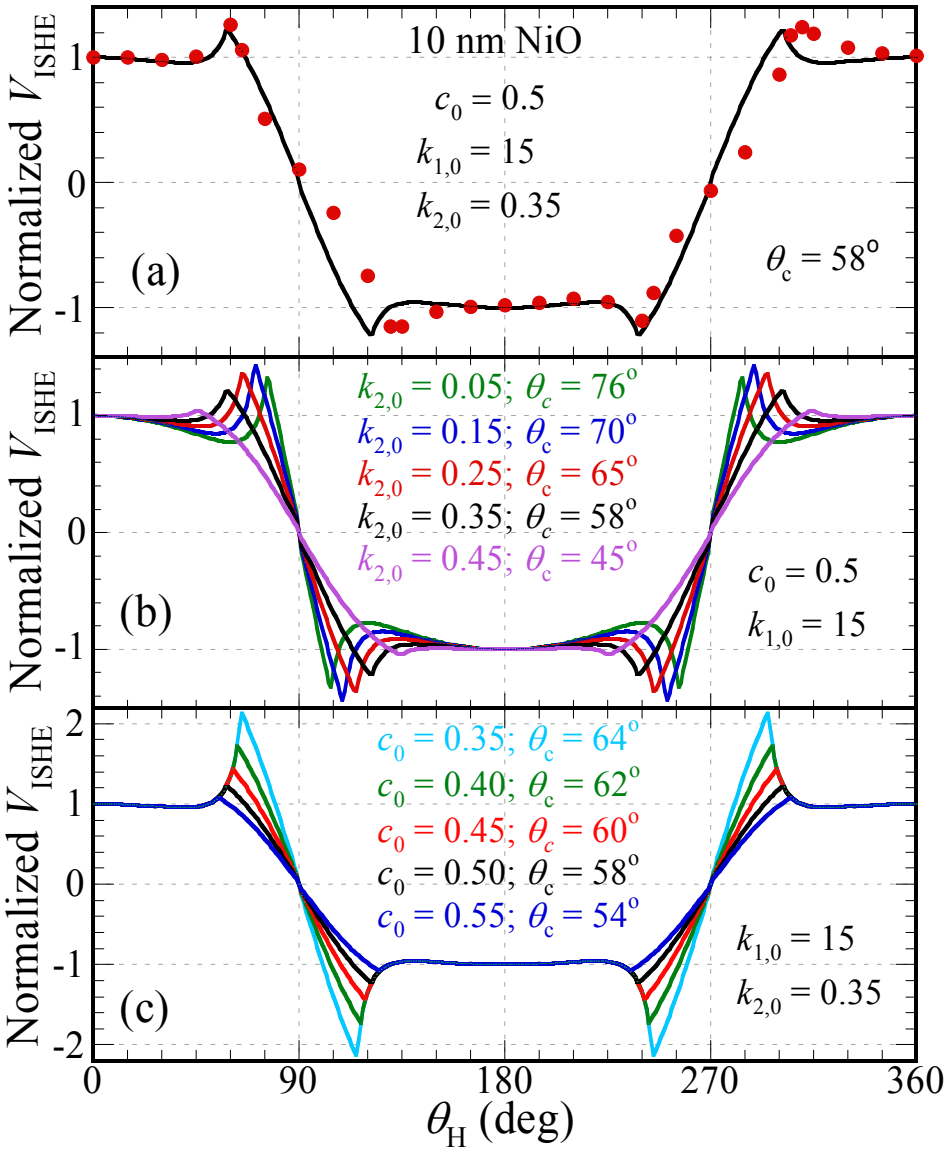
10 nm NiO
c_0 = 0.5
$k_{1,0}$ = 15
$k_{2,0}$ = 0.35
θ_c = 58°
(a)
Normalized V_{ISHE}
$k_{2,0}$ = 0.05; θ_c = 76°
$k_{2,0}$ = 0.15; θ_c = 70°
$k_{2,0}$ = 0.25; θ_c = 65°
$k_{2,0}$ = 0.35; θ_c = 58°
$k_{2,0}$ = 0.45; θ_c = 45°
c_0 = 0.5
$k_{1,0}$ = 15
(b)
Normalized V_{ISHE}
c_0 = 0.35; θ_c = 64°
c_0 = 0.40; θ_c = 62°
c_0 = 0.45; θ_c = 60°
c_0 = 0.50; θ_c = 58°
c_0 = 0.55; θ_c = 54°
$k_{1,0}$ = 15
$k_{2,0}$ = 0.35
(c)
Normalized V_{ISHE}
0
90
180
270
360
θ_H (deg)

Figure 5.